

# Fast 360° 3D Metrology for Directed Energy Deposition

James Taylor<sup>1</sup>, Jiazhang Wang<sup>1,\*</sup>, Guanzhong Hu<sup>2</sup>, Zihan Chen<sup>2</sup>, Ping Guo<sup>2</sup>, and Florian Willomitzer<sup>1,\*</sup>

<sup>1</sup>Wyant College of Optical Sciences, University of Arizona, Tucson, AZ, USA

<sup>2</sup>Department of Mechanical Engineering, Northwestern University, Evanston, IL, USA

\*Correspondence: jiazhangwang@arizona.edu ; fwillomitzer@arizona.edu

## Abstract

Directed Energy Deposition (DED) is a metal additive manufacturing process capable of building and repairing large, complex metal parts from a wide range of alloys. Its flexibility makes it attractive for multiple industrial applications, e.g., in aerospace, automotive and biomedical fields. However, errors or defects introduced at any stage of the printing process can, if undetected, significantly impact the final result, rendering the printed part unusable. Potential in-situ correction methods of printing defects require fast and high-resolution on-the-fly 3D inspection inside the machine, but existing 3D monitoring methods often lack full 360° 3D coverage, require bulky setups, or are too slow for real-time layer-wise feedback. In this paper, we present a single-shot, multi-view polarized fringe projection profilometry (FPP) system designed for real-time in-situ 3D inspection during DED printing. Multiple camera-projector pairs are arranged around the deposition surface to measure depth from different viewpoints in single-shot, while cross-polarized image filtering suppresses specular reflections caused by varying surface reflectance across different alloys. The final 360° reconstruction is obtained via joint registration of the captured multi-view measurements. Our prototype has been deployed in a DED system and our first experiments demonstrate a depth precision better than  $\delta z < 50\mu m$  on partially reflective and "shiny" metal surfaces, enabling accurate, layer-wise monitoring for closed-loop DED control.

## 1. Introduction

Directed Energy Deposition (DED) [1–3] is a powerful metal additive manufacturing process that uses a focused energy source, typically a high-power laser, to create a melt pool into which metallic powder or wire is continuously fed. This forms beads that are stacked layer by layer to fabricate parts with complex geometries and tailored microstructures. Unlike powder bed fusion (PBF) methods [4, 5], DED is open-architecture, highly scalable, and capable of depositing material onto existing components, making it particularly suited for larger builds, multi-material fabrication, and on-the-fly repair applications in aerospace, energy, automotive, and tooling industries [6, 7].

The nascent field of DED printing and processing introduces significant new metrology challenges that differ fundamentally from those in PBF, where the powder bed provides

a relatively uniform, diffuse surface that can be easily measured by conventional optical metrology methods. In contrast, DED surfaces typically show mixed surface reflectance properties and have a "shiny" appearance. These surface types are particularly hard to measure for common optical 3D sensors, as most sensor principles are fundamentally limited [8, 9] to either purely diffuse [10] or purely specular surfaces [11–13]. Moreover, the DED-produced surface shapes are rough, irregular, and highly dynamic due to localized heating and rapid solidification, all of which can lead to defects such as porosity, lack of fusion, and geometric distortion. These defects may form unpredictably and accumulate over time, underscoring the need for in-situ layer-wise geometric monitoring. Several optical monitoring strategies have attempted to address this need [14–16]. For instance, the authors of [14] utilized a CCD camera to observe the side profile of the growing build and adjusted the deposition height based on the silhouette contours. While this approach enables basic feedback control, it is fundamentally limited to two-dimensional profiles. The complex material interactions and rapidly evolving topography of DED, however, often results in steep slopes, deep melt tracks and complex surfaces, requiring a "full" 3D measurement for process control.

The authors of [15] later introduced a laser line scanner to evaluate the part's surface topography during DED, demonstrating the ability to detect surface deviations. However, single-line scanners inherently suffer from low 3D data density and require a multitude of camera images. For instance, obtaining a "full" or "pixel-dense" 3D model with a 1 Megapixel camera ( $1000pix \times 1000pix$ ) would require about 1000 camera images which need to be sequentially captured while the line is scanned over the object [17, 18].

Fringe Projection Profilometry (FPP) [10, 19, 20] is typically the gold standard for measuring dense and highly accurate 3D data of diffuse surfaces, but the conventional temporal phase-shifting approach of fringe patterns also requires to capture a temporal sequence of fringe images. This means that for both of these techniques, the object is not allowed to move or change during the measurement period, which significantly increases the total DED printing time and system complexity, and makes related approaches unsuitable for fast in-process monitoring where thermal dynamics evolve rapidly. Moreover, most standard active triangulation techniques (like FPP or line triangulation) are, as discussed, not well suited to measure shiny metallic surfaces without further

modification, and are prone to artifacts caused by specular reflection highlights. Effective geometric monitoring of DED therefore demands a method that can handle surfaces with varying reflectance properties, combined with high-speed acquisition.

Another important factor for effective DED monitoring is achieving comprehensive 360° coverage of the printed part simultaneously from all viewing angles, which, to our knowledge, has not been demonstrated in prior work. Instead, current monitoring approaches are limited to one specific viewing direction, which is in many cases insufficient for DED, where steep sidewalls, overhangs, and the presence of the deposition head frequently cause occlusions that hide critical regions. Achieving the required comprehensive coverage is technically challenging: the confined chamber volume restricts sensor placement; illumination and imaging hardware must be carefully calibrated across multiple viewpoints; and residual specular reflections and registration errors can easily degrade data quality. Overcoming these barriers requires both hardware optimization and algorithmic strategies for calibration, synchronization, and robust fusion of overlapping views.

In this paper, we introduce a full 360° 3D measurement system that employs a single-shot FPP strategy based on Fourier Transform Profilometry (FTP) [21, 22]. FTP delivers dense 3D measurements, but unlike traditional phase-shifted FPP, it requires the capture of only one single camera image to calculate one 3D image, which significantly speeds up the acquisition time. To measure mixed reflectance metallic surfaces with high precision, we apply cross-polarization filtering that filters out unwanted specular lobes. Our system integrates multiple camera–projector pairs distributed 360° around the build plate, each acquiring the surface from a distinct perspective. The measurements are then jointly registered into a unified 3D reconstruction, enabling synchronized, full-field capture from all viewpoints. This architecture supports high-throughput, layer-wise geometric inspection with precision, compatible with the real-time requirements of in-situ DED processes. We summarize our contributions as follows:

- A compact, multi-view, single-shot fringe projection profilometry (FPP) system designed specifically for 360° in-situ DED monitoring.
- Integration of high-speed depth acquisition, polarization-based reflectance control, and a registration pipeline that selectively fuses multiple views via normal-based correspondence filtering.
- Validation on complex metallic parts inside a production DED chamber, as well as on designated test objects demonstrating a precision better than  $\delta z < 50\mu m$  in single-shot.
- First steps towards a scalable foundation for next-generation, closed-loop 360° metrology in DED additive manufacturing.

## 2. Methods

We introduce an in-situ, 360° 3D imaging system for precise and fast surface measurement in DED. The system is based on Fringe Projection Profilometry (FPP) and is specifically tailored to meet the unique challenges of measuring metallic object surfaces in DED environments. To this end, our used methods integrate multiple imaging and reconstruction techniques, including single-shot phase evaluation, joint system calibration, 3D feature-based multi-view surface registration, and polarization filtering. The following subsections provide a detailed description of each component.

**2A. DED principle and hardware.** The DED hardware used in this paper is the Additive Rapid Prototyping Instrument (ARPI) [23], a laser power blown DED system (see Fig. 1). The ARPI deposition chamber ( $\sim 650mm \times 500mm \times 300mm$ ) accommodates two critical components:

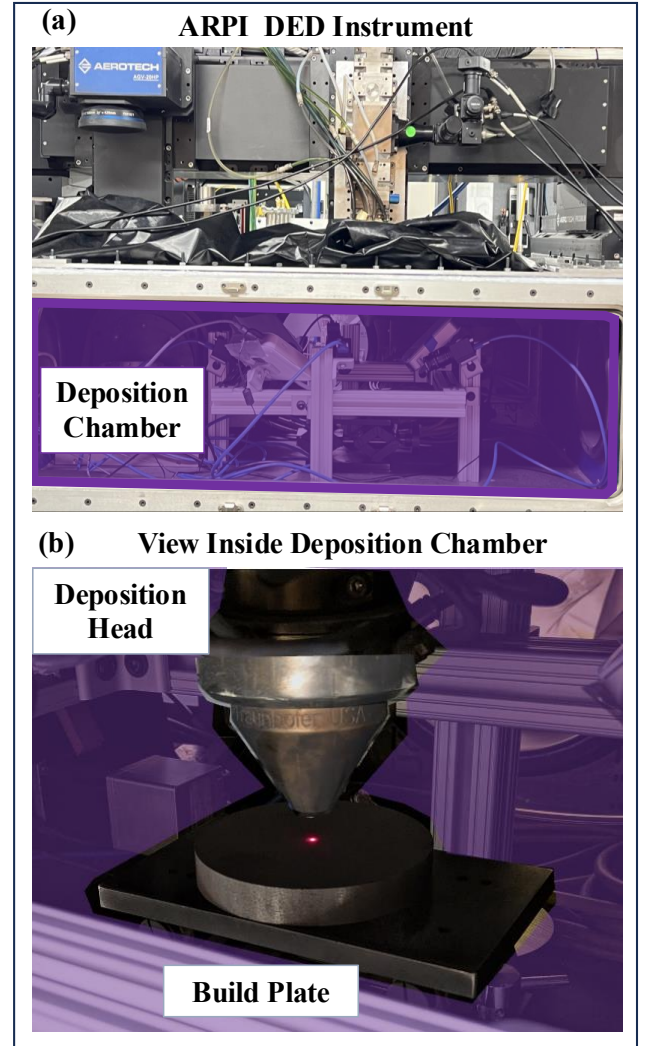


**Fig. 1.** Directed Energy Deposition (DED) chamber and hardware. (a) The full ARPI system with the deposition chamber highlighted in purple, indicating the rough dimensions ( $\sim 650mm \times 500mm \times 300mm$ ) into which our multi-view measurement system must fit. (b) Interior view of the chamber showing the two key components, deposition head and build plate, relevant to both DED functionality and the design of our multi-view system.

the deposition head and the build plate (see Fig. 1(b)). The deposition head integrates a high-power laser with a coaxial powder delivery system, ensuring uniform melting and deposition. Powder flow is carefully regulated through adjustable gas-driven nozzles, enabling precise control over deposition rates and geometric accuracy. The build plate serves as the substrate upon which material deposition occurs. Precise control of the deposition head's translation, rotation and overall trajectory allows complex geometries to be fabricated layer by layer. This integrated DED system provides robust control over the deposition process, enabling the production of metallic parts with tailored microstructures and optimized geometrical features for demanding industrial and research applications.

**2B. In-situ 360° FPP system and calibration.** Fringe Projection Profilometry (FPP) is a widely used optical metrology technique that enables accurate and dense optical 3D surface reconstruction by analyzing the deformation of light patterns. A calibrated projector projects a known sinusoidal fringe pattern onto the object surface, which is observed with a camera under a triangulation angle  $\theta$ . Due to the shape variations of the object surface, the fringes appear deformed in the camera image (see Fig. 2). This deformation, quantified as a variation in the local phase  $\varphi$  of the observed pattern, is used to calculate the depth profile of the object. To relate the captured fringe deformation to the actual 3D geometry of the measured surface, a phase-

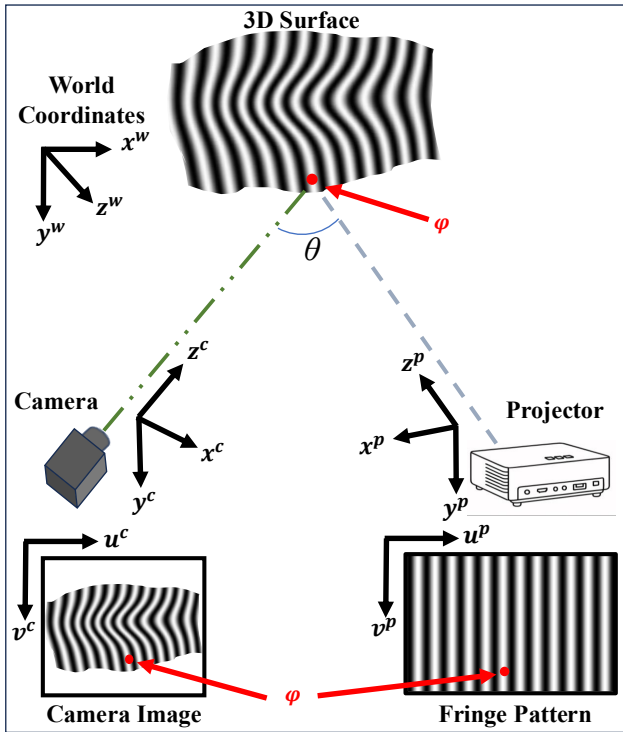


**Fig. 2.** Schematic of a calibrated FPP system, where a camera images the deformation of a projected fringe pattern. A representative point on the surface (shown in red) illustrates how the phase information  $\varphi$  of the scene establishes the correspondence between camera  $(u^c, v^c)$  and projector  $(u^p, v^p)$  pixels. From this correspondence, the known geometry between projector and camera can be used to triangulate the depth of the scene.

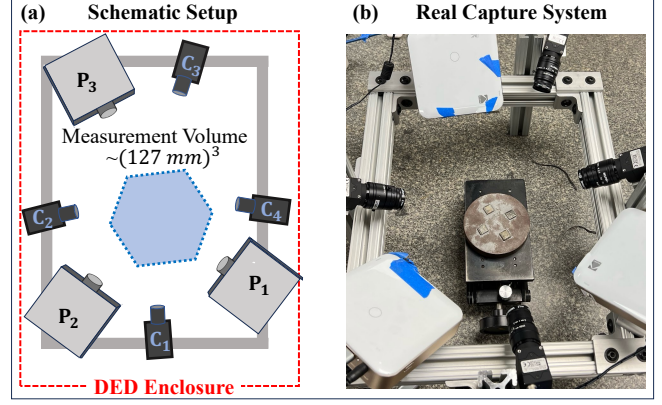


**Fig. 3.** 360° multi-view system. (a) The schematic image of the system shows the arrangement of multiple FPP sub-sensors around the defined measurement volume. While fitting inside the DED deposition chamber, the cameras and projectors are also positioned to avoid obstructing any of the ARPI internal mechanisms. (b) Image of the real capture system placed outside the DED chamber.

correspondence must be established between each camera and projector pixel. Obtaining two corresponding points in camera image and projector image then allows for 3D point reconstruction via triangulation (see Fig. 2). In conventional systems, the fringe phase in each pixel (which establishes correspondence) is typically obtained via temporal phase-shifting techniques [19, 20], where the projector sequentially displays several phase-shifted fringe patterns. One of the most common approaches is the so-called four-step phase-shifting algorithm [19], in which four fringe images with relative phase shifts of  $\pi/2$  are utilized. As these multi-shot techniques are not used to capture 3D data in our system, we defer to [17, 24–27] for more information about phase shifting FPP.

In contrast to standard FPP systems, our proposed 360° FPP system uses a fast single-shot acquisition approach (described in sec. 2D) and consists of multiple camera-projector pairs, each representing an independent FPP sub-sensor. Our current prototype system consists of four monochrome cameras and three digital projectors arranged around the DED build plate (see Fig. 3). Although this results in theoretically 12 independent FPP sub-sensors, the actual number of used pairs varies with application and printing geometry. For most examples shown in this paper, we utilized 3-4 FPP sub-sensors. Each pair is modeled and calibrated using the pinhole camera approximation: A 3D point is defined as  $\mathbf{X}^w = [x^w, y^w, z^w, 1]^T$  in world coordinates (see Fig. 2), and is mapped onto the respective camera and projector chip (image plane) via their respective intrinsic and extrinsic parameters.

We first calibrate each camera independently using a planar checkerboard target, following Zhang's method [28]. Multiple images of the calibration board are acquired at varied poses inside the measurement volume, and sub-pixel precise corner locations are extracted. The camera intrinsics  $\mathbf{K}$  and lens distortion coefficients are estimated using a nonlinear optimization procedure, which minimizes the reprojection error between observed and projected checker corners across all frames [29]. The projectors in our system are cal-



ibrated in the same way, i.e., by treating each projector as an inverse camera [30]. Since a projector cannot directly observe the calibration board, we project phase shifted sinusoids onto the calibration board to establish correspondence between camera and projector for each checkerboard position. Eventually, we can obtain the exact projector pixel coordinate for each observed checker corner, effectively allowing the projector to "see" the board through the calibrated camera. Given this procedure, we estimate the intrinsic matrix  $\mathbf{K}$  and extrinsic pose  $[\mathbf{R}|\mathbf{T}]$  of each projector in each FPP sub-sensor by minimizing the reprojection error, analogous to the camera calibration procedure.

After calibrating each camera and projector individually, the final step is to establish a common reference frame across all four cameras. This requires estimating the relative poses (extrinsics) of the cameras with respect to each other. To this end, we capture multiple images of the same planar checkerboard at varied poses, ensuring that all four cameras observe the calibration board simultaneously. Sub-pixel accurate corner detections are extracted in each view and used to constrain the camera poses into a shared coordinate system. Eventually, the extrinsic parameters—namely the rotation  $\mathbf{R}_c$  and translation  $\mathbf{T}_c$  of each camera—are jointly optimized to minimize the reprojection error of all checkerboard corners across all FPP sub-sensors [31]. After choosing Camera 1's coordinates as joint "reference frame", the multi-view system is calibrated to reconstruct  $360^\circ$  3D scenes.

**2C. Specular-diffuse separation via multi-view polarization filtering.** The "shiny" reflectance properties of metallic surfaces, common with DED, present a significant challenge for most active triangulation principles (including FPP), as these methods are designed for matte lambertian surfaces [9, 32]. When imaging metallic glossy surfaces, extended specular lobes from directed reflections can saturate image sensors and introduce large errors and artifacts in the captured 3D point cloud [33]. To mitigate this effect and mainly capture the diffuse part of the light signal which is back scattered from the metallic surface, we ap-

ply cross-polarization filtering [34]. As specular reflection preserves the polarization state of the incident light, while diffuse scattering scrambles the polarization state, polarization filtering can be employed to selectively suppress the unwanted specular component. Consequently, we add a linear polarizer in front of each projector to define the polarization state of the emitted light. The corresponding camera in each FPP sub-sensor is then equipped with a second linear polarizer, oriented exactly to filter out the directly reflected light that maintained its polarization state when reflected off the metallic surface.

To demonstrate and evaluate the effect of polarization filtering on our measurements, we performed a controlled comparison on a shiny metallic test part under identical illumination and viewing geometry. Figure 4(a) shows a raw fringe image acquired without polarization filtering and the corresponding 3D reconstruction. Several regions exhibit strong specular highlights, with saturated pixel values that corrupt the underlying sinusoidal pattern information. As expected, these saturated zones lead to significant artifacts in the resulting 3D reconstruction. Moreover, due to the large dynamic range of the scene, some image regions are too dark to obtain a signal with sufficient SNR, leading to increased noise in the respective 3D reconstruction. In contrast, Fig. 4(b) shows the corresponding fringe image acquired under the cross-polarized configuration. It can be seen that the majority of specular glare is effectively suppressed, and high SNR fringe visibility is preserved across a large area of the object surface. The resulting 3D reconstruction demonstrates significantly improved continuity and surface fidelity, with no visible artifacts.

We note that our multi-view arrangement can further improve this approach by mitigating the few remaining surface points where saturation occurs. Some specular reflections can still be present after polarization filtering. This is because the cameras' filters only remove light whose polarization is along a specific axis which is most likely to block light from direct reflection. Accordingly, incident polarized light along a different axis may still arrive on the sensor. This can occur as

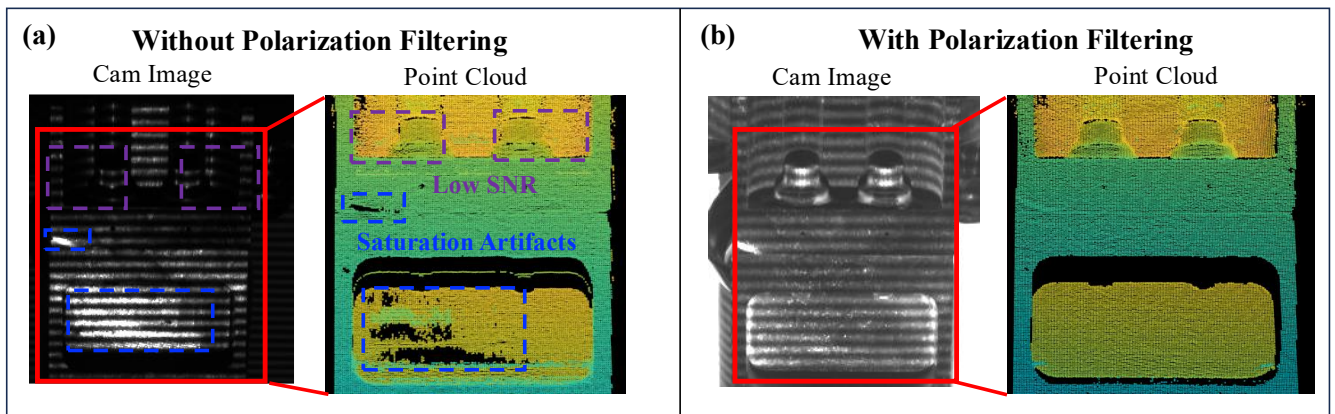


**Fig. 4.** Specular-diffuse separation via polarization filtering. (a) Example measurement without polarization filtering. The camera image frame shows a visible degraded fringe pattern signal such as strong saturation due to specular reflection and regions with low SNR. The corresponding regions in the evaluated 3D point cloud show distinct artifacts or strong noise. (b) Same measurement with specular reflections suppressed by polarization filtering. The fringe pattern is homogeneously visible in the image frame, with a better signal throughout the measurement surface.

a result of inter-reflections or complex surface geometry, and the specular component from this reflection is not effectively suppressed. Because these "unfavorable" reflections are dependent on viewing angle, they are likely not present for the same surface point observed from a different camera position. So if there are remaining sparse saturated regions for one camera, a camera at a different position with an overlapping view will observe an uncorrupted signal from this surface area. During the multi-view registration and normal-based fusion process discussed in sec. 2F, the corrupted 3D data is then replaced by the artifact-free data from the other viewpoint.

**2D. Single-shot FPP measurements.** Traditional FPP techniques rely on the projection of a temporal series of phase-stepped patterns, meaning that a temporal sequence of multiple camera images needs to be captured to calculate one single 3D image. As discussed, this multi-shot acquisition can become problematic for dynamic or unstable measurement environments in DED, where even slight motion or thermal fluctuations between frames can lead to reconstruction artifacts. To ensure motion robustness of each captured 3D view, we adopt a specific flavor of FPP (based on Fourier Transform Profilometry (FTP) [21, 22]), which can be performed in single-shot, i.e., only requires one single camera image to calculate one 3D view. In FTP, a high-frequency sinusoidal fringe pattern is projected onto the object surface and a single camera image (such as shown in Fig. 5(a)) is captured. The recorded sinusoidal intensity distribution can be expressed as

$$I(x, y) = a(x, y) + b(x, y) \cos(2\pi f_0 x + \varphi(x, y)) \quad (1)$$

where  $a(x, y)$  is bias illumination,  $b(x, y)$  is modulation amplitude,  $f_0$  is carrier frequency, and  $\varphi(x, y)$  is object-encoded phase, which is used to determine the correspondence. We apply a two-dimensional Fourier transform to separate this into a DC term and first-order lobes, as illustrated in Fig. 5(b)

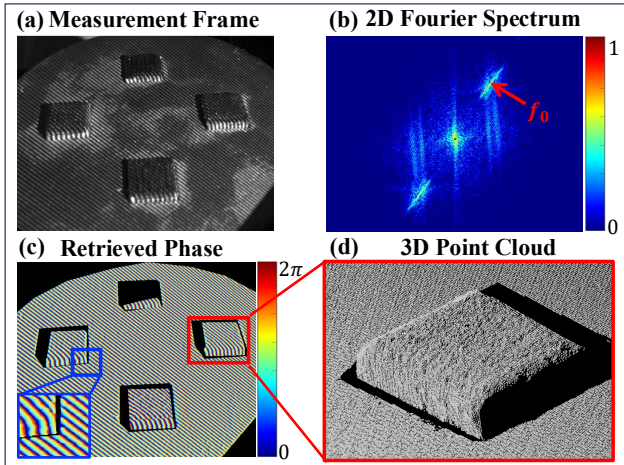


**Fig. 5.** Single-shot FPP (FTP) 3D measurement pipeline: (a) Raw captured fringe image. (b) Fourier spectrum. (c) Obtained wrapped phase map. (d) Final 3D reconstruction.

$$\mathcal{F}\{I(x, y)\} = A(f_x, f_y) + B(f_x - f_0, f_y) + B^*(f_x + f_0, f_y) \quad (2)$$

These lobes are aligned around the respective carrier frequency and contain a copy of the object spectrum. We use a Hanning band-pass filter [35] to isolate one first-order lobe, and apply an inverse Fourier transform to obtain the wrapped phase map of our sinusoidal camera image:

$$\varphi(x, y) = \arg[\mathcal{F}^{-1}\{B(f_x - f_0, f_y)\}] \quad (3)$$

shown in Fig. 5(c). The wrapped phase must then be unwrapped to obtain a continuous phase distribution across the surface, needed to calculate the 3D coordinates. This can be done by a variety of strategies, such as reference markers, a known reference surface like the build plate, or stereo correspondence between multiple views [17]. For the examples shown in this paper, we use the build plate (which is seen by all cameras) as a reference surface. The so-obtained final phase and correspondence map is then used to calculate the 3D point cloud of the surface (see Fig. 5(d)) via triangulation (see Fig. 2).

**2E. Quantitative evaluation of 3D data precision.** The precision of active triangulation measurements is influenced by several system parameters, such as triangulation angle  $\theta$ , lateral camera resolution or SNR. Understanding the interplay of all involved parameters is key for a physical optimization of the hardware setup [9], meaning that the resulting tradeoff-space can be optimized towards a specific goal (e.g., high speed, large FoV, etc.), which is dictated by the targeted application. We refer to [9, 17] for an overview of involved limits and tradeoffs.

For a quantitative precision evaluation of our proposed FPP system, we performed controlled 3D measurements on objects with well-defined geometries. To emulate the measurement scenario as realistic as possible, we measured a metallic planar object (the build plate) inside the DED chamber. The precision of the measured point cloud was then quantified by fitting a low frequency polynomial surface to the reconstructed point cloud and then calculating the root-mean-square error (RMSE) of the residual point distances between the measured 3D points and the best-fit surface. We performed this procedure for our single-shot FPP (FTP) method described in sec. 2D and, for comparison, also for the standard multi-shot FPP method. Importantly, as triangulation angle and other system parameters slightly vary for each FPP sub-sensor, we performed this evaluation for all 4 commonly used FPP sub-sensors in our multi-view system. The evaluated precision values  $\delta z$  have been quantified between  $37.4\mu\text{m}$  and  $43.6\mu\text{m}$  (mean value  $\delta z_{\text{mean}} = 40.3\mu\text{m}$ ) for single-shot and  $28.4\mu\text{m}$  to  $48.4\mu\text{m}$  (mean value  $\delta z_{\text{mean}} = 35.5\mu\text{m}$ ) for the multi-shot phase-shifting FPP comparison, meaning that our introduced single-shot setup reaches sub-50 $\mu\text{m}$  precision in all 4 FPP sub-system.

**2F. multi-view registration and normal-based point-cloud fusion.** To achieve complete 360° coverage of the



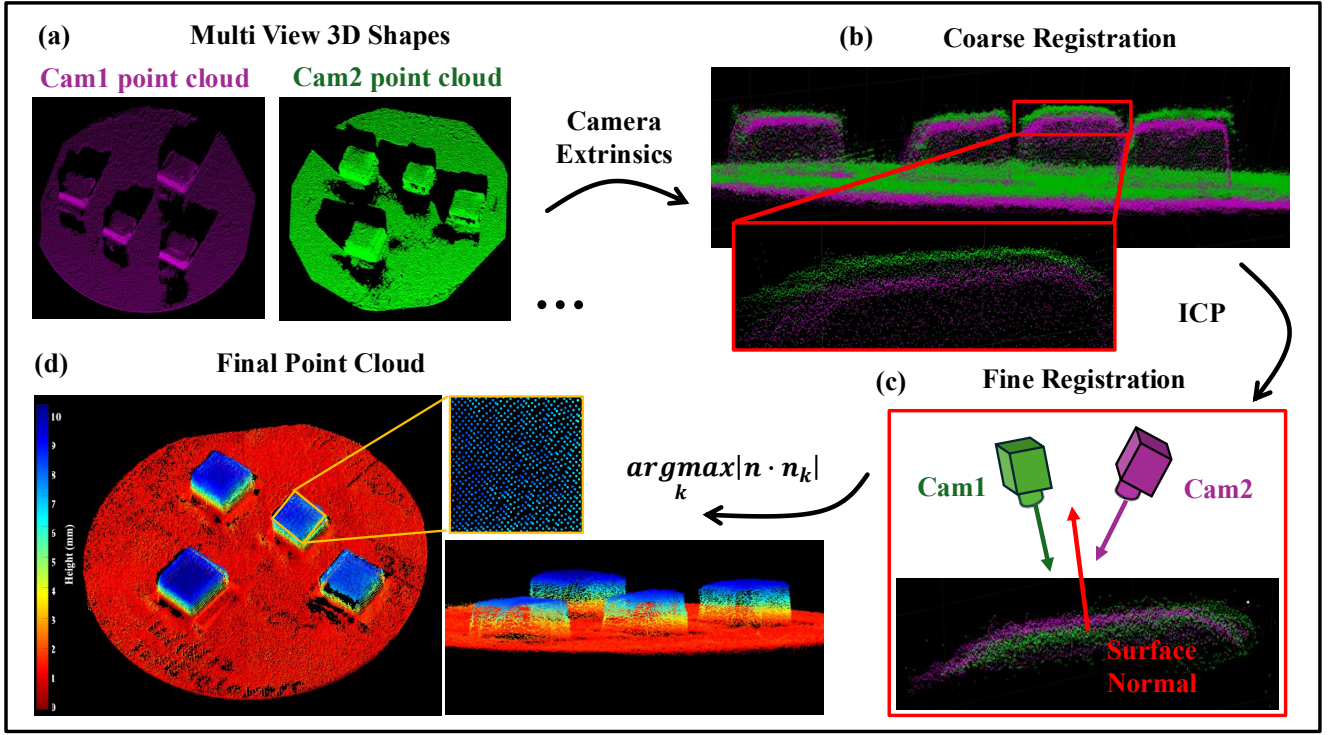


**Fig. 6.** Multi-view point cloud fusion (example with two views): (a) Reconstruct 3D point clouds from two different viewpoints. (b) Perform coarse alignment using calibrated camera extrinsics; a noticeable gap remains between the two point clouds. (c) Apply fine alignment via Iterative Closest Point (ICP) to minimize inter-cloud discrepancies. (d) Compute the angle between the surface normal and each camera's optical axis, and retain the point cloud from the camera with the smaller angular deviation. The fused reconstruction reveals clear surface ripples on the object.

object geometry, the partial reconstructions from each FPP sub-system must be accurately registered into a unified coordinate system. This is accomplished through a two-stage registration pipeline consisting of an initial coarse alignment followed by a fine alignment and view fusion step.

In the first stage, all views are transformed into the coordinate frame of Camera 1 using the calibration parameters obtained during system calibration and joint pose optimization (see sec. 2B). An example point cloud is shown in Fig. 6(b).

However, due to inevitable remaining calibration inaccuracies, an additional fine registration stage is required. For this, we first identify overlapping regions in the point clouds from the different captured 3D views. These regions are observed across multiple cameras, and can be identified using a combination of build plate visibility information and surface segmentation based on local surface normals calculated from the respective point clouds. Once the overlapping surfaces are identified, we perform an Iterative Closest Point (ICP) [36–38] alignment between the identified overlap regions. The result before and after the ICP is shown in Fig. 6(b) and (c). It can be seen that the different point clouds are now largely overlapping in one surface.

Following the ICP multi-view registration, multiple views from multiple FPP sub-sensors may contribute redundant measurements in overlapping regions. This can pose a challenge for fine high-frequency surface features, such as "hatch ripples" [39]: Remaining registration errors can lead to small translations or rotations between each multi-view point cloud, effectively "washing out" fine features. To address this

potential issue, we implement a surface normal-based filtering strategy that retains only the most reliable point cloud for each overlap region that is assumed to provide the highest quality data. For each set of overlapping regions, we take the computed set of surface normals, and compare their angle with the position and direction of each camera's optical axis. The quality metric for a given surface patch is then inferred from the relative angle between mean normal vector  $\mathbf{n}$  (see Fig. 6(c)) and the camera's optical axis  $\mathbf{n}_k$ , defined as the  $z$ -axis in each camera's frame, i.e.,  $[0, 0, 1]^T$ . Points observed under more direct (i.e., near-normal) viewing angles are assumed to deliver higher quality point clouds and are

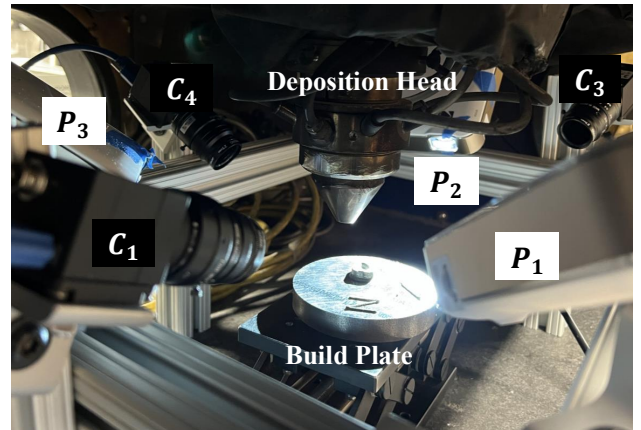


**Fig. 7.** Our 360° 3D metrology system inside the DED chamber.

prioritized, as these are less affected by oblique perspective distortion and are more likely to preserve fine geometric features. All other overlapping point clouds are discarded. The final 360° reconstruction retains only points from the “best-viewed” point clouds. This view-selective fusion ensures high-fidelity surface representation and preserves local blurring from multi-view redundancy. The result is a complete and geometrically consistent 360° point cloud (Fig. 6(d)), constructed from the best portions of each view without introducing blending artifacts.

### 3. In-situ Measurement Results and Evaluation

To validate the proposed system under realistic conditions, we deployed the full 360° metrology setup inside the functional DED machine described in sec. 2A. The multi-view system shown in Fig. 3 was designed to both fit inside the chamber while avoiding any possible obstruction with moving internal parts. Our system consists of four 2 Megapixel cameras (FLIR BFS-U3-19S4M) equipped with 8 mm objective lenses and three projectors (Kodak Luma 350) arranged around the measurement volume. The projectors are positioned with approximately 120 degree angular separation, enabling full coverage of the target volume. The cameras are similarly arranged, and an additional fourth camera is present to allow for additional 3D information to be obtained from each projector. Figure 7 shows the complete assembly mounted on a modular aluminum frame and placed inside the DED chamber.

The following results demonstrate and evaluate our sys-

tem’s performance for different imaging scenarios: fast single-shot 3D reconstruction from one FPP sub-system and 360° multi-view reconstruction and registration of a complicated part from 3 FPP sub-systems.

**3A. In-situ single-shot 3D measurements.** The first set of experiments demonstrates the sensitivity of our single-shot method (described in sec. 2D) to single layer DED depositions. We acquire single-shot FPP measurements of the metallic “balloon dog” print, shown in Fig. 8 at multiple stages of the printing process. Figure 8 shows the 3D reconstruction before (Fig. 8(a)), and after (Fig. 8(b)) the deposition of one additional layer. The point cloud overlays clearly reveal localized height changes corresponding to the deposited regions while maintaining stable geometry in surrounding areas. A depth profile drawn across the deposition zone (Fig. 8(d)) shows a distinct offset the two layer states, which is in accordance with the nominal interlayer steps during the printing process [16].

We further validate our method on a taller DED-built part with many accumulated layers (Fig. 9). The 3D point cloud (Fig. 9(b)) taken from the side of the part shows that our single-shot method nicely captures different deposition layers. A height map (Fig. 9(c)) and line profile along the side surface (Fig. 9(c)) reveals the structure of the deposited layers, where each hump corresponds to one DED pass. These results demonstrate that the system not only detects subtle single-layer increments but also resolves stacked layer profiles in taller builds with high fidelity.

We emphasize again that these results present single-shot measurements from one FPP sub-system, and no registration

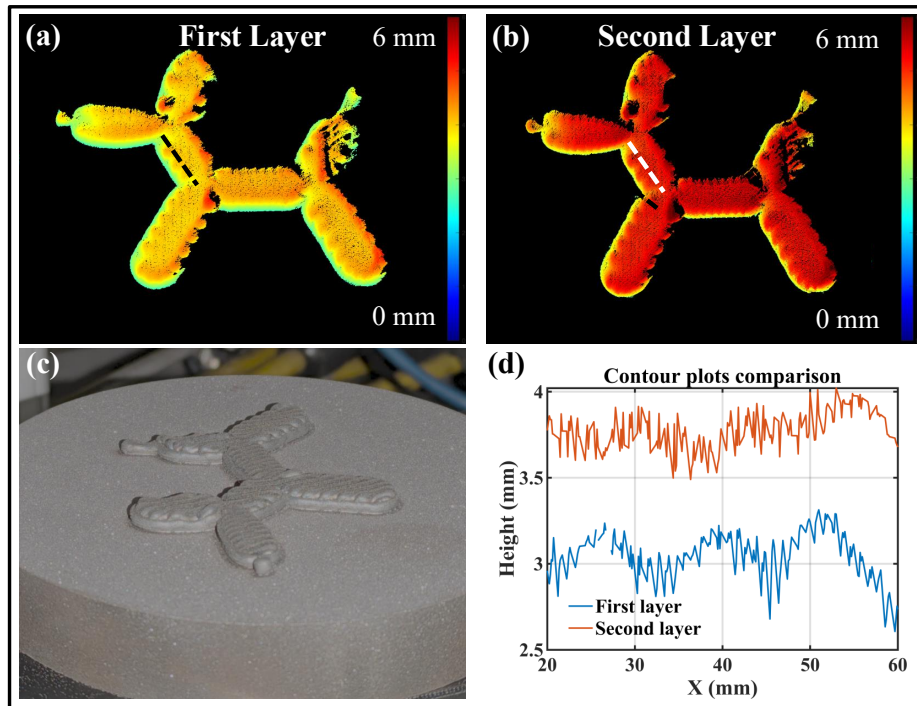


**Fig. 8.** In-situ measurement of single-layer DED deposition with fast single-shot FPP. Two layers of a “balloon dog” are subsequently printed on a build plate. (a) Height map after printing the first layer. (b) Height map after printing the second layer. (c) Image of “balloon dog” part that is being measured. (d) Height profiles along the black and white lines drawn in both (a) and (b), respectively. Height difference between two layers as well as hatch ripples can be resolved.

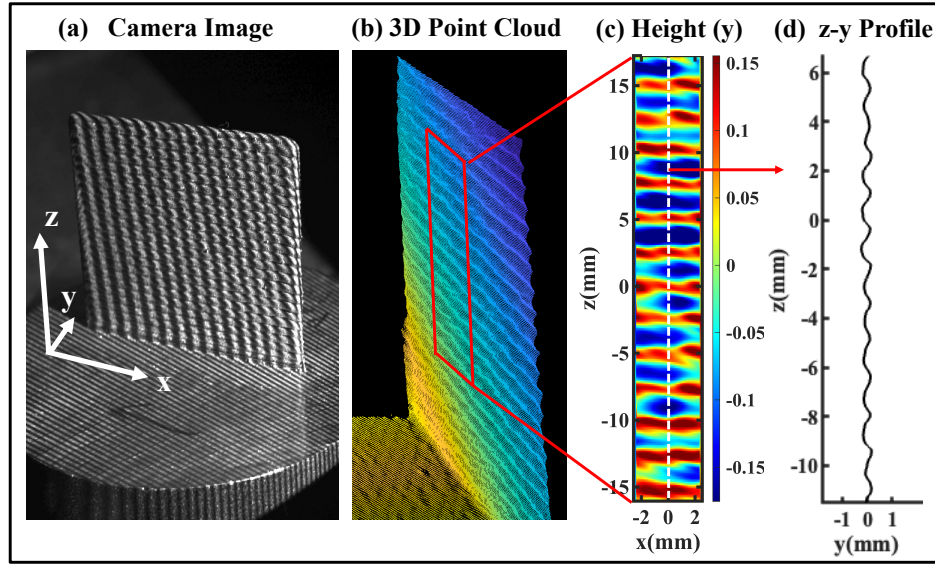


**Fig. 9.** In-situ single-shot FPP measurement of a tall DED part. (a) Camera Image. (b) Evaluated 3d point cloud, showing the side of the part. Different deposition layers can be clearly seen. (c) Height map of the side profile. (d) z-y profile plot to visualize deposition layers.

of different 3D point clouds has been applied. The total time (including acquisition and time to evaluate the 3D model) is below 0.5 seconds. This means that, even without further algorithmic optimization, our prototype system is already able to continuously monitor fast 3D printing processes in specific regions of the object on-the-fly, without requiring lengthy interruptions of the printing process during the measurement.

**3B. In-situ 360° multi-view measurement of a complicated part.** To evaluate the robustness of our registration algorithm, we performed a full in-situ 360° measurement of the same metallic part (see Fig. 9(a)) whose single point cloud view was evaluated in sec. 3A. The object consists of a single printed thin wall. This geometry of two closely spaced planar surfaces separated only by the wall thickness presents a particularly challenging task for multi-view registration algorithms, and conventional Iterative Closest Point (ICP) align-

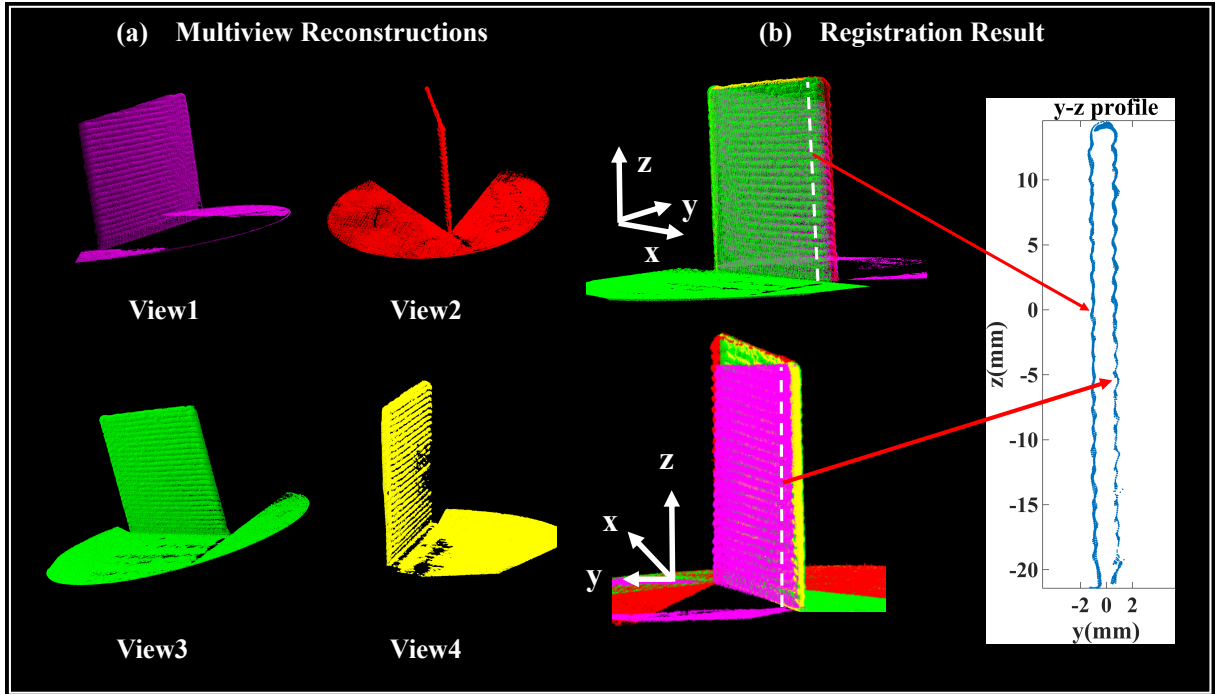


**Fig. 10.** In-situ 360° 3D measurement of a printed thin wall part. (a) Individual 3D point clouds from the 4 FPP sub-sensors used in this measurement. (b) Two views of the final registration result. Using the baseplate as an XY plane, a height profile is plotted along the white dashed lines in the final point cloud, showing a representative cross section of our surface reconstruction. The thin wall geometry presents a unique challenge to conventional ICP registration as the two closely spaced wall surfaces could be registered together. Due to our surface normal-based detection of overlap regions in the individual pointclouds, our registration algorithm is robust to this error and can reconstruct the thin wall object with its true thickness in high quality.



ment is highly prone to error in such cases: because ICP minimizes point-to-point Euclidean distances, the standard approach tends to collapse two nearly parallel planes into a single surface, effectively erasing the true wall thickness. The result would be an incorrect 3D model where opposing wall surfaces are spuriously merged.

For the 360° measurement shown in Fig. 10, we collect four individual point clouds from four FPP sub-sensors. Figure 10(a) shows the four individual point clouds prior to registration. Each point cloud contains only part of the structure, and, as the figure illustrates, the thin wall produces three planar point clusters (view 1,3, and 4) that lie in close proximity. As discussed, our developed registration algorithm addresses this challenge by exploiting surface normal information to determine valid overlap regions (see sec. 2F). In the specific case of thin walls, opposing cameras view surfaces whose normals are nearly antiparallel are explicitly rejected as candidate overlaps and the respective parts of the point clouds are not ICP registered to each other. The benefit of this strategy is evident in Fig. 10(b). After registration, the four partial reconstructions are fused into a unified model that preserves the distinct geometry of each wall surface. A representative cross-section (Fig. 10(b) right) taken along the dashed lines in the figure confirms that the reconstructed profile maintains the true thickness of the wall, with no spurious collapse into a single plane. This experiment demonstrates that our normal-based registration produces stable and accurate results even in scenarios that are challenging for ICP-based methods. More broadly, it highlights the ability of the approach to preserve fine structures and prevent topological errors in multi-view 3D reconstruction of multilayer DED structures.

## Discussion and Outlook

We presented a fast and precise 360° 3D metrology system for in-situ DED monitoring. The presented results demonstrate that our system enables single-shot, high-precision 360° metrology of shiny metallic printed parts inside the DED chamber. By combining single shot FPP (FTP) with cross-polarization filtering, the approach effectively suppresses specular reflections and captures surface geometry with sufficient sensitivity to resolve both single-layer changes and stacked layer profiles, at depth precisions better than  $\delta z < 50\mu m$ . Our multi-view registration further extends coverage, allowing partial reconstructions to be fused into a complete point cloud while mitigating residual specular saturation through complementary viewpoints. We see our prototype system as a first step towards dynamic, in-situ DED monitoring and inspection where motion and thermal instabilities make approaches relying on long measurement sequences less practical.

Our system, however, is not without limitations: although each FPP sub-sensor captures the object surface in single-shot, a multi-view measurement that uses multiple projectors still relies on a short image sequence that cycles through all used projectors. While we condone this fact for our first proof-of-principle prototype, future version of our system

could address this limitation by, e.g., color projection and filtering or other multiplexing schemes to achieve fully single-shot multi-view measurements. Our other work will focus on optimizing system timing and acquisition speed to further improve robustness and throughput, enabling broader deployment in industrial additive manufacturing environments.

We hope that our system will enable novel printing and monitoring capabilities that could even go beyond DED, facilitating faster, more robust and more accurate additive manufacturing techniques in the future.

**Acknowledgements:** This research was supported by the National Science Foundation under Grant number CMMI-2216298.

## References

- [1] David Svetlizky, Mitun Das, Baolong Zheng, Alexandra L. Vyatskikh, Susmita Bose, Amit Bandyopadhyay, Julie M. Schoenung, Enrique J. Lavernia, and Noam Eliaz. Directed energy deposition (ded) additive manufacturing: Physical characteristics, defects, challenges and applications. *Materials Today*, 49:271–295, 2021.
- [2] Adrita Dass and Atieh Moridi. State of the art in directed energy deposition: From additive manufacturing to materials design. *Coatings*, 9(7):418, 2019.
- [3] DR Feenstra, R Banerjee, HL Fraser, A Huang, A Molotnikov, and Nick Birbilis. Critical review of the state of the art in multi-material fabrication via directed energy deposition. *Current Opinion in Solid State and Materials Science*, 25(4):100924, 2021.
- [4] Wayne E King, Andrew T Anderson, Robert M Ferencz, Neil E Hodge, Chandrika Kamath, Saad A Khairallah, and Alexander M Rubenchik. Laser powder bed fusion additive manufacturing of metals: physics, computational, and materials challenges. *Applied Physics Reviews*, 2(4), 2015.
- [5] Riya Singh, Akash Gupta, Ojastez Tripathi, Sashank Srivastava, Bharat Singh, Ankita Awasthi, S Kumar Rajput, Pankaj Sonia, Piyush Singhal, and Kuldeep K Saxena. Powder bed fusion process in additive manufacturing: An overview. *Materials Today: Proceedings*, 26:3058–3070, 2020.
- [6] David Svetlizky, Mitun Das, Baolong Zheng, Alexandra L. Vyatskikh, Susmita Bose, Amit Bandyopadhyay, Julie M. Schoenung, Enrique J. Lavernia, and Noam Eliaz. Directed energy deposition (ded) additive manufacturing: Physical characteristics, defects, challenges and applications. *Materials Today*, 49:271–295, 2021. ISSN 1369-7021. doi: <https://doi.org/10.1016/j.matmod.2021.03.020>.
- [7] Abdollah Saboori, Alberta Aversa, Giulio Marchese, Sara Biamino, Mariangela Lombardi, and Paolo Fino. Application of directed energy deposition-based additive manufacturing in repair. *Applied Sciences*, 9(16), 2019. ISSN 2076-3417. doi: 10.3390/app9163316.
- [8] Gerd Häusler and Svenja Ettl. Limitations of optical 3d sensors. In *Optical measurement of surface topography*, pages 23–48. Springer, 2011.
- [9] Gerd Häusler and Florian Willomitzer. Reflections about the holographic and non-holographic acquisition of surface topography: where are the limits? *Light: Advanced Manufacturing*, 3(2):226–235, 2022.
- [10] Jing Xu and Song Zhang. Status, challenges, and future perspectives of fringe projection profilometry. *Optics and Lasers in Engineering*, 135:106193, 2020.
- [11] Jiazhang Wang, Oliver Cossairt, and Florian Willomitzer. 3d imaging of complex specular surfaces by fusing polarimetric and deflectometric information. *Optica*, 12(4):446–450, 2025.
- [12] Markus C Knauer, Jurgen Kaminski, and Gerd Häusler. Phase measuring deflectometry: a new approach to measure specular free-form surfaces. In *Optical Metrology in Production Engineering*, volume 5457, pages 366–376. SPIE, 2004.
- [13] Jiazhang Wang, Tianfu Wang, Bingjie Xu, Oliver Cossairt, and Florian Willomitzer. Accurate eye tracking from dense 3d surface reconstructions using single-shot deflectometry. *Nature Communications*, 16(1):2902, 2025.
- [14] Alireza Fathi, Amir Khajepour, Ehsan Toyserkani, and Mohammad Durali. Clad height control in laser solid freeform fabrication using a feedforward pid controller. *The International Journal of Advanced Manufacturing Technology*, 35:280–292, 12 2007. doi: 10.1007/s00170-006-0721-1.
- [15] Lequn Chen, Xiling Yao, Peng Xu, Seung Moon, and Guijun Bi. Rapid surface defect identification for additive manufacturing with in-situ point cloud processing and machine learning. *Virtual and Physical Prototyping*, 16, 10 2020. doi: 10.1080/17452759.2020.1832695.
- [16] Guanzhong Hu, Ruijing Zha, Yaoke Wang, Jian Cao, and Ping Guo. Digital fringe projection for interlayer print defect characterization in directed energy deposition. In *International Symposium on Flexible Automation*, volume 87882, page V001T01A002. American Society of Mechanical Engineers, 2024.
- [17] Florian Willomitzer. *Single-Shot 3D Sensing Close to Physical Limits and Information Limits*. Springer, 2019.
- [18] Florian Willomitzer and Gerd Häusler. Single-shot 3d motion picture camera with a dense point cloud. *Optics express*, 25(19):23451–23464, 2017.
- [19] V. Srinivasan, H. C. Liu, and M. Hallioui. Automated phase-measuring profilometry of 3-d diffuse objects. *Appl. Opt.*, 23(18):3105–3108, Sep 1984. doi: 10.1364/AO.23.003105.
- [20] Chao Zuo, Shijie Feng, Lei Huang, Tianyang Tao, Wei Yin, and Qian Chen. Phase shifting algorithms for fringe projection profilometry: A review. *Optics and lasers in engineering*, 109:23–59, 2018.

- [21] Mitsuo Takeda and Kazuhiro Mutoh. Fourier transform profilometry for the automatic measurement of 3-d object shapes. *Applied optics*, 22(24):3977–3982, 1983.
- [22] Xianyu Su and Wenjing Chen. Fourier transform profilometry:: a review. *Optics and Lasers in Engineering*, 35(5):263–284, 2001.
- [23] Center for Advanced Optics, Northwestern University. Facilities – center for advanced optics. <https://www.cao.mech.northwestern.edu/facilities/>, 2025.
- [24] Shijie Feng, Chao Zuo, Liang Zhang, Tianyang Tao, Yan Hu, Wei Yin, Jiaming Qian, and Qian Chen. Calibration of fringe projection profilometry: A comparative review. *Optics and Lasers in Engineering*, 143:106622, 2021. ISSN 0143-8166. doi: <https://doi.org/10.1016/j.optlaseng.2021.106622>.
- [25] Kai Liu, Yongchang Wang, Daniel L Lau, Qi Hao, and Laurence G Hassebrook. Dual-frequency pattern scheme for high-speed 3-d shape measurement. *Optics express*, 18(5): 5229–5244, 2010.
- [26] Basel Salahieh, Zhenyue Chen, Jeffrey J. Rodriguez, and Rongguang Liang. Multi-polarization fringe projection imaging for high dynamic range objects. *Opt. Express*, 22(8):10064–10071, Apr 2014. doi: 10.1364/OE.22.010064.
- [27] Florian Willomitzer, Chia-Kai Yeh, Vikas Gupta, William Spies, Florian Schiffrers, Aggelos Katsaggelos, Marc Walton, and Oliver Cossairt. Hand-guided qualitative deflectometry with a mobile device. *Optics Express*, 28(7):9027–9038, 2020.
- [28] Z. Zhang. A flexible new technique for camera calibration. *IEEE Transactions on Pattern Analysis and Machine Intelligence*, 22(11):1330–1334, 2000. doi: 10.1109/34.888718.
- [29] J. Heikkilä and O. Silven. A four-step camera calibration procedure with implicit image correction. In *Proceedings of IEEE Computer Society Conference on Computer Vision and Pattern Recognition*, pages 1106–1112, San Juan, Puerto Rico, 1997. IEEE Computer Society.
- [30] Daniel Moreno and Gabriel Taubin. Simple, accurate, and robust projector-camera calibration. In *2012 Second International Conference on 3D Imaging, Modeling, Processing, Visualization & Transmission*, pages 464–471. IEEE, 2012.
- [31] Alberto J. Perez, Juan-Carlos Perez-Cortes, and Jose-Luis Guardiola. Simple and precise multi-view camera calibration for 3d reconstruction. *Computers in Industry*, 123:103256, 2020. ISSN 0166-3615. doi: <https://doi.org/10.1016/j.compind.2020.103256>.
- [32] Aniket Dashpute, Jiazhang Wang, James Taylor, Oliver Cossairt, Ashok Veeraraghavan, and Florian Willomitzer. Event-based motion-robust accurate shape estimation for mixed reflectance scenes. *arXiv preprint arXiv:2311.09652*, 2023.
- [33] H. Zhang, C. K. Prasad Vallabh, and X. Zhao. Machine learning enhanced high dynamic range fringe projection profilometry for in-situ layer-wise surface topography measurement during lpb additive manufacturing. *ASME Journal of Manufacturing Science and Engineering*, 2023. © 2024 by ASME.
- [34] Tongbo Chen, Hendrik PA Lensch, Christian Fuchs, and Hans-Peter Seidel. Polarization and phase-shifting for 3d scanning of translucent objects. In *2007 IEEE conference on computer vision and pattern recognition*, pages 1–8. IEEE, 2007.
- [35] Ralph Beebe Blackman and John Wilder Tukey. The measurement of power spectra from the point of view of communications engineering—part i. *Bell System Technical Journal*, 37(1):185–282, 1958.
- [36] Paul J Besl and Neil D McKay. Method for registration of 3-d shapes. In *Sensor fusion IV: control paradigms and data structures*, volume 1611, pages 586–606. Spie, 1992.
- [37] Oliver Arold, Svenja Ettl, Florian Willomitzer, and Gerd Häusler. Hand-guided 3d surface acquisition by combining simple light sectioning with real-time algorithms. *arXiv preprint arXiv:1401.1946*, 2014.
- [38] Florian Willomitzer, Svenja Ettl, Oliver Arold, and Gerd Häusler. Flying triangulation—a motion-robust optical 3d sensor for the real-time shape acquisition of complex objects. In *AIP Conference Proceedings*, volume 1537, pages 19–26. American Institute of Physics, 2013.
- [39] B. Guan. Laser polishing of directed energy deposition metal parts. *Journal of Manufacturing Science and Engineering*, page —, 2024. doi: 10.1115/1.4054755. Overlapping scans modify ripple frequency distribution, affecting surface roughness.